Computers & Fluids 38 (2009) 1528–1538

Contents lists available at ScienceDirect

Computers & Fluids

journal homepage: www.elsevier.com/locate/compfluid

Continuous adjoint approach to the Spalart–Allmaras turbulence model for incompressible flows

A.S. Zymaris [a], D.I. Papadimitriou [a], K.C. Giannakoglou [a,*], C. Othmer [b]

[a] National Technical University of Athens, School of Mechanical Engineering, Parallel CFD & Optimization Unit, P.O. Box 64069, 15710 Athens, Greece
[b] Volkswagen AG, CAE Methods, Group Research, Letter Box 1777, D-38436 Wolfsburg, Germany

ARTICLE INFO

Article history:
Received 7 July 2008
Received in revised form 15 December 2008
Accepted 16 December 2008
Available online 25 December 2008

ABSTRACT

A continuous adjoint formulation for the computation of the sensitivities of integral functions used in steady-flow, incompressible aerodynamics is presented. Unlike earlier continuous adjoint methods, this paper computes the adjoint to both the mean-flow and turbulence equations by overcoming the frequently made assumption that the variation in turbulent viscosity can be neglected. The development is based on the Spalart–Allmaras turbulence model, using the adjoint to the corresponding differential equation and boundary conditions. The proposed formulation is general and can be used with any other integral function. Here, the continuous adjoint method yielding the sensitivities of the total pressure loss functional for duct flows with respect to the normal displacements of the solid wall nodes is presented. Using three duct flow problems, it is demonstrated that the adjoint to the turbulence equations should be taken into account to compute the sensitivity derivatives of this functional with high accuracy. The so-computed derivatives almost coincide with "reference" sensitivities resulting from the computationally expensive direct differentiation. This is not, however, the case of the sensitivities computed without solving the turbulence adjoint equation, which deviates from the reference values. The role of all newly appearing terms in the adjoint equations, their boundary conditions and the gradient expression is investigated, significant and insignificant terms are identified and a study on the Reynolds number effect is included.

1. Introduction

In aerodynamic shape optimization methods, given (a) an objective function J, (b) a set of N design variables ($b_n, n = 1, \ldots, N$; in most cases, these are shape controlling parameters, though flow parameters can also be among them) and (c) the governing (flow/state) equations, the adjoint method computes the gradient of J with respect to b_n, i.e. sensitivity derivatives $\frac{\delta J}{\delta b_n}$. A key advantage of the adjoint method is that these derivatives are computed at cost comparable to that of numerically solving the state p.d.e.'s.

The discrete adjoint equations can be derived through either the continuous, [1–7], or the discrete adjoint approach, [8–11,20]. In the continuous approach, the adjoint equations are derived as p.d.e.'s and, then, discretized. In the discrete approach, the discrete adjoint equations result from the discretized state equations. The continuous adjoint approach allows understanding the physical significance of the adjoint equations and boundary conditions. It also offers flexibility in choosing the discretization scheme for the adjoint equations which may differ from that used for the state p.d.e.'s but may result to discrepancies in the gradient of the discretized objective function. The discrete adjoint provides the exact gradient of the discrete objective function and ensures that the optimization process can fully converge. It, however, suffers from increased memory requirements and, in case of high-order discretization schemes with extended stencils, the development cost increases noticeably. It is beyond the scope of this paper to discuss further these advantages and disadvantages; in the limit of infinite grid resolution and for smooth solutions both approaches are consistent and converge to the correct value of the gradient, [21,31]. Note that the present paper is exclusively concerned with the continuous approach.

In continuous adjoint, the development starts from the augmented objective function L, defined as the sum of J and the field (Ω) integral of the residual of the state equations ($R_i = 0$) multiplied by the adjoint variables (ψ_i); thus, $L = J + \int_\Omega \psi_i R_i \, d\Omega$. The variation of the L is made independent of variations in state variables by satisfying appropriate adjoint equations and boundary conditions, giving rise to expressions for the sensitivity derivatives in terms of the computed ψ_i fields. Since J is an integral, the sensitivity derivatives are expressed as boundary and/or field integrals, depending on the type of J and the adjoint formulation. In inverse design problems, for instance, where J is an integral along the solid walls, formulations leading to sensitivity derivatives with, [2,12,3,5], or without, [13–15,6], field integrals can be found. A more subtle approach is needed when J includes line (in 2D)/surface (in 3D) integrals along

* Corresponding author. Tel.: +30 210 772 1636; fax: +30 210 772 1658.
E-mail address: kgianna@central.ntua.gr (K.C. Giannakoglou).

0045-7930/$ - see front matter © 2008 Elsevier Ltd. All rights reserved.
doi:10.1016/j.compfluid.2008.12.006

the inlet and outlet, which are not directly affected by the shape controlling parameters. This is the case of the function expressing total pressure losses, as shown by the authors in [16] for compressible flows. Here, the same function is used for incompressible flows. Note that one may extend this method to field integrals, such as that of entropy generation presented in [17,18].

In turbulent flows, the mean-flow equations are coupled with the turbulence model one(s) and both must be considered as state equations. The adjoint approach should take into account variations in the mean-flow and turbulence variables. However, the literature survey, [3,6,7,12] reveals that the latter are often neglected. In the so-called frozen turbulence assumption $\left(\frac{\delta \nu_t}{\delta b_n}=0\right)$, the mathematical development is less tedious, the expressions for $\frac{\delta J}{\delta b_n}$ are simpler and there is no need to solve additional p.d.e.'s for the turbulence adjoint variables; however, as it will be demonstrated below, the resulting sensitivity derivatives may deviate from the exact ones. The scope of this paper is to set up a continuous adjoint approach for the entire system of state p.d.e.'s (mean-flow equations and the Spalart–Allmaras model equation, [19]), derive exact expressions for $\frac{\delta J}{\delta b_n}$ and quantify the error introduced by neglecting the turbulence adjoint terms in selected examples.

To the authors' knowledge, such a continuous adjoint approach is new. A few similar works that take into account variations in turbulent viscosity can only be reported, but these are all based on the discrete adjoint approach. For instance, Nielsen et al. [23] present a discrete adjoint method for the compressible mean flow equations tightly coupled with the Spalart–Allmaras model, which preserves discrete duality and achieves asymptotic convergence behavior equivalent to that of the flow problem. Zingg et al. [25] solve the system of state and discrete adjoint equations (including linearization of the coupled turbulence model) using the same preconditioned Krylov method, aiming at faster and more reliable convergence. Dwight and Brezillon [26] present a discrete adjoint to an unstructured finite-volume solver for the RANS; the adjoint is based on the full linearization of all terms in the solver, including all turbulence model (Spalart–Allmaras–Edwards) contributions. In the same paper, the reader may find a detailed classification of the approximations which are often used when the exact adjoint to the turbulence equations is to be avoided. Anderson and Bonhaus [22] also present a discrete adjoint approach on unstructured grids where the Spalart–Allmaras model is strongly coupled with the flow equations and the accuracy of derivatives is demonstrated through comparison with finite differences. Lee and Kim [24] present a discrete adjoint method for the compressible RANS coupled with the k–ω SST model, for subsonic S-shaped intake geometries; the adjoint solver is parallelized to offset the extra cost for solving the two turbulent adjoint equations. The discrete adjoint of the complete optimization problem, including flow equations and mesh motion, where the linearization takes into account the full coupling of flow and turbulence equations, is shown in [27]. A detailed feasibility study of the usually made constant eddy-viscosity assumption in gradient-based optimization, by focusing on the discrete adjoint method, is presented in [28]. Compared to all the previously mentioned works, the present paper differs in that the continuous, rather than the discrete, adjoint is developed; the development produces physically significant adjoint p.d.e.'s and boundary conditions. Note, also, that the present paper deals with the incompressible steady-state flow equations and applications are restricted to duct flows.

It should become clear that the scope of this paper is to present a (continuous adjoint) method to compute accurate derivatives of flow-related functionals, not necessarily for the purpose of driving a descent method to the optimal solution. In engineering applications, the knowledge of sensitivity derivatives of an aerodynamic shape can be used to draw the designer's attention to components that are susceptible to further improvement. However, to avoid any misunderstanding, we should make clear that this paper does not intend to convince the reader that gradient-based optimization methods must necessarily be supported by the exact gradient. It is well known that many efficient optimization methods are driven by gradient approximations. As shown below, this paper demonstrates that, depending on the Reynolds number, the omission of solving the adjoint to the turbulence model equation(s) may damage the accuracy of the computed gradient. In addition, by means of the numerical investigation of the role of all new terms (in the adjoint equations, their boundary conditions and the gradient expression), one by one, we may identify more or less significant terms before deciding about simplifications to be made.

2. Flow model

The flow model consists of the Navier–Stokes equations for incompressible fluid flows and the Spalart–Allmaras one-equation turbulence model. The mean-flow equations are written as

$$R_{U,i}=v_j\frac{\partial v_i}{\partial x_j}+\frac{\partial p}{\partial x_i}-\frac{\partial}{\partial x_j}\left[(\nu+\nu_t)\left(\frac{\partial v_i}{\partial x_j}+\frac{\partial v_j}{\partial x_i}\right)\right]=0,\quad i=1,2,3 \tag{1}$$

$$R_{U,4}=\frac{\partial v_j}{\partial x_j}=0 \tag{2}$$

where v_i (velocity components) and p (static pressure) stand for the mean-flow state variables. According to the Einstein convention, repeated indices imply summation. Neglecting the transition term, the Spalart–Allmaras turbulence model [19] reads

$$R_{\tilde{\nu}}=\frac{\partial\left(v_j\tilde{\nu}\right)}{\partial x_j}-\frac{\partial}{\partial x_j}\left[\left(\nu+\frac{\tilde{\nu}}{\sigma}\right)\frac{\partial\tilde{\nu}}{\partial x_j}\right]-\frac{c_{b2}}{\sigma}\left(\frac{\partial\tilde{\nu}}{\partial x_j}\right)^2-\tilde{\nu}P(\tilde{\nu})+\tilde{\nu}D(\tilde{\nu})=0 \tag{3}$$

where $\tilde{\nu}$ is the turbulence state variable. The eddy viscosity coefficient ν_t is expressed in terms of $\tilde{\nu}$ as follows:

$$\nu_t=\tilde{\nu}f_{\nu_1} \tag{4}$$

The production and destruction terms in Eq. (3) read

$$P(\tilde{\nu})=c_{b1}\tilde{S},\quad D(\tilde{\nu})=c_{w1}f_w(\tilde{S})\frac{\tilde{\nu}}{d^2} \tag{5}$$

where $\tilde{S}=S+\frac{\tilde{\nu}}{d^2\kappa^2}f_{\nu_2}$, $S=|e_{ijk}\frac{\partial v_k}{\partial x_j}\vec{i}_i|$ is the vorticity magnitude, e_{ijk} is the permutation symbol, d the distance from the wall, $f_{\nu_1}=\frac{\chi^3}{\chi^3+c_{\nu_1}^3}$, $f_{\nu_2}=1-\frac{\chi}{1+\chi f_{\nu_1}}$, $\chi=\frac{\tilde{\nu}}{\nu}$, $f_w=g\left(\frac{1+c_{w_3}^6}{g^+c_{w_3}^6}\right)^{1/6}$, $g=r+c_{w_2}(r^6-r)$ and$r=\frac{\tilde{\nu}}{\tilde{S}\kappa^2d^2}$. The constants are $c_{b1}=0.1355$, $c_{b2}=0.622$, $\kappa=0.4187$, $\sigma=\frac{2}{3}$, $c_{w1}=\frac{c_{b1}}{\kappa^2}+\frac{(1+c_{b2})}{\sigma}$, $c_{w2}=0.3, c_{w3}=2$, $c_{v1}=7.1$ and $c_{v2}=5$.

The mean-flow equations are solved on structured grids in a segregated manner, by employing the SIMPLE algorithm [29]. A collocated, cell-centered storage of flow variables is used. Numerical dissipation is introduced by computing the pressure gradients at the pressure equation directly at each face center of a control volume. Convection terms are modeled using a second-order upwind scheme. The system of the discretized equations is solved using the preconditioned (through the biconjugate gradient stabilized, CGSTAB, algorithm; see [30]) conjugate gradient method.

3. Continuous adjoint approach – basic development

In this section, the continuous adjoint method producing the sensitivities $\frac{\delta J}{\delta b_n}$ is developed in a general manner without considering a specific function J or specific shape controlling parameters b_n. By introducing the adjoint (or costate, ψ_i) variables u_i, q and $\tilde{\nu}_a$,

associated with the v_i, p and $\tilde{\nu}$, respectively, the variation in the augmented function L is written as

$$\frac{\delta L}{\delta b_n} = \frac{\delta J}{\delta b_n} + \int_\Omega u_i \frac{\partial R_{U,i}}{\partial b_n}\, d\Omega + \int_\Omega q \frac{\partial R_{U,4}}{\partial b_n}\, d\Omega + \int_\Omega \tilde{\nu} \frac{\partial R_{\tilde{\nu}}}{\partial b_n}\, d\Omega \tag{6}$$

where Ω is the flow domain with boundary Γ. In Eq. (6), a sharp distinction must be made between global (symbol δ) and direct (symbol ∂) variations and the corresponding sensitivity derivatives. By varying b_n, the locations of grid nodes vary too. Thus, the global variation in any quantity Φ is expressed as the sum of direct and grid-dependent variations, namely

$$\frac{\delta \Phi}{\delta b_n} = \frac{\partial \Phi}{\partial b_n} + \frac{\partial \Phi}{\partial x_k}\frac{\delta x_k}{\delta b_n} \tag{7}$$

The use of direct derivatives in Eq. (6) allows the permutation of $\frac{\partial}{\partial x_k}$ and $\frac{\partial}{\partial b_n}$ (i.e. $\frac{\partial}{\partial x_k}\left(\frac{\partial \Phi}{\partial b_n}\right) = \frac{\partial}{\partial b_n}\left(\frac{\partial \Phi}{\partial x_k}\right)$), see [6], which would not be the case if the global variation was used instead (in general, $\frac{\partial}{\partial x_i}\left(\frac{\delta \Phi}{\delta b_n}\right) \neq \frac{\delta}{\delta b_n}\left(\frac{\partial \Phi}{\partial x_i}\right)$). The direct derivatives of the state equations (mean-flow and turbulence equations; Eqs. (2)–(5)) with respect to b_n are given by

$$\begin{aligned}\frac{\partial R_{U,i}}{\partial b_n} = {} & \frac{\partial v_j}{\partial b_n}\frac{\partial v_i}{\partial x_j} + v_j \frac{\partial}{\partial x_j}\left(\frac{\partial v_i}{\partial b_n}\right) + \frac{\partial}{\partial x_i}\left(\frac{\partial p}{\partial b_n}\right) \\ & - \frac{\partial}{\partial x_j}\left\{(\nu + \nu_t)\left[\frac{\partial}{\partial x_j}\left(\frac{\partial v_i}{\partial b_n}\right) + \frac{\partial}{\partial x_i}\left(\frac{\partial v_j}{\partial b_n}\right)\right]\right\} \\ & - \frac{\partial}{\partial x_j}\left[\frac{\partial \nu_t}{\partial b_n}\left(\frac{\partial v_i}{\partial x_j} + \frac{\partial v_j}{\partial x_i}\right)\right] = 0, \quad i = 1,2,3\end{aligned} \tag{8}$$

$$\frac{\partial R_{U,4}}{\partial b_n} = \frac{\partial}{\partial x_j}\left(\frac{\partial v_j}{\partial b_n}\right) \tag{9}$$

where the bulk viscosity ν is assumed constant whereas

$$\frac{\partial \nu_t}{\partial b_n} = \frac{\delta \nu_t}{\delta \tilde{\nu}}\frac{\partial \tilde{\nu}}{\partial b_n} \tag{10}$$

and

$$\begin{aligned}\frac{\partial R_{\tilde{\nu}}}{\partial b_n} = {} & \underbrace{\frac{\partial}{\partial x_j}\left(\frac{\partial v_j}{\partial b_n}\tilde{\nu}\right) + \frac{\partial}{\partial x_j}\left(v_j \frac{\partial \tilde{\nu}}{\partial b_n}\right)}_{term1} \underbrace{- \frac{\partial}{\partial x_j}\left[\left(\nu + \frac{\tilde{\nu}}{\sigma}\right)\frac{\partial}{\partial x_j}\left(\frac{\partial \tilde{\nu}}{\partial b_n}\right)\right]}_{term2} \\ & \underbrace{- \frac{1}{\sigma}\frac{\partial}{\partial x_j}\left(\frac{\partial \tilde{\nu}}{\partial b_n}\frac{\partial \tilde{\nu}}{\partial x_j}\right)}_{term3} \underbrace{- 2\frac{c_{b2}}{\sigma}\frac{\partial \tilde{\nu}}{\partial x_j}\frac{\partial}{\partial x_j}\left(\frac{\partial \tilde{\nu}}{\partial b_n}\right)}_{term4} \\ & \underbrace{+ \tilde{\nu}\left(-\frac{\partial P}{\partial b_n} + \frac{\partial D}{\partial b_n}\right)}_{term5} \underbrace{+ (-P + D)\frac{\partial \tilde{\nu}}{\partial b_n}}_{term6}\end{aligned} \tag{11}$$

By assuming that the variations in turbulence quantities with respect to b_n are zero (i.e. the widely made assumption; see [12,3,6,7]), Eqs. (8), (9) and (7) (with $\Phi = v_i$ or p), yield

$$\begin{aligned}& \int_\Omega \left(u_i \frac{\partial R_{U,i}}{\partial b_n} + q\frac{\partial R_{U,4}}{\partial b_n}\right) d\Omega \\ & = \int_\Gamma \left[u_j v_j n_i + u_i v_j n_j + (\nu + \nu_t)\frac{\partial u_i}{\partial x_j}n_j - q n_i\right]\frac{\partial v_i}{\partial b_n}\, d\Gamma \\ & \quad - \int_\Gamma (\nu + \nu_t)\frac{\partial}{\partial x_j}\left(\frac{\partial v_i}{\partial b_n}\right) n_j u_i\, d\Gamma + \int_\Omega \left\{-v_j\left(\frac{\partial u_j}{\partial x_i} - \frac{\partial u_i}{\partial x_j}\right)\right. \\ & \quad \left. - \frac{\partial}{\partial x_j}\left[(\nu + \nu_t)\left(\frac{\partial u_i}{\partial x_j} + \frac{\partial u_j}{\partial x_i}\right)\right] + \frac{\partial q}{\partial x_i}\right\}\frac{\partial v_i}{\partial b_n}\, d\Omega + \int_\Gamma u_j n_j \frac{\partial p}{\partial b_n}\, d\Gamma \\ & \quad - \int_\Omega \frac{\partial u_j}{\partial x_j}\frac{\partial p}{\partial b_n}\, d\Omega\end{aligned} \tag{12}$$

In the present paper, we focus on the new terms arising by neglecting the "frozen turbulence viscosity" assumption. If $\frac{\partial \nu_t}{\partial b_n}$ is not neglected, the last term in Eq. (8) contributes the additional term

$$\begin{aligned}- \int_\Omega u_i \frac{\partial}{\partial x_j}\left[\frac{\partial \nu_t}{\partial b_n}\left(\frac{\partial v_i}{\partial x_j} + \frac{\partial v_j}{\partial x_i}\right)\right] d\Omega = {} & - \int_\Gamma \frac{\delta \nu_t}{\delta \tilde{\nu}} u_i \left(\frac{\partial v_i}{\partial x_j} + \frac{\partial v_j}{\partial x_i}\right) n_j \frac{\partial \tilde{\nu}}{\partial b_n}\, d\Gamma \\ & + \int_\Omega \frac{\delta \nu_t}{\delta \tilde{\nu}}\frac{\partial u_i}{\partial x_j}\left(\frac{\partial v_i}{\partial x_j} + \frac{\partial v_j}{\partial x_i}\right)\frac{\partial \tilde{\nu}}{\partial b_n}\, d\Omega\end{aligned} \tag{13}$$

to the r.h.s. of Eq. (12). The derivative $\frac{\delta \nu_t}{\delta \tilde{\nu}}$ is analytically computed using the Spalart–Allmaras model equations.

The integral $\int_\Omega \tilde{\nu}\frac{\partial R_{\tilde{\nu}}}{\partial b_n}\, d\Omega$, that appears in Eq. (6), after substituting Eq. (11) for $\frac{\partial R_{\tilde{\nu}}}{\partial b_n}$, becomes on a term-by-term basis (n_j are the components of the outward unit normal vector along Γ)

$$\begin{aligned}term1: \quad & \int_\Omega \tilde{\nu}_a\left[\frac{\partial}{\partial x_j}\left(\frac{\partial v_j}{\partial b_n}\tilde{\nu}\right) + \frac{\partial}{\partial x_j}\left(v_j\frac{\partial \tilde{\nu}}{\partial b_n}\right)\right] d\Omega \\ & = \int_\Gamma \tilde{\nu}_a \tilde{\nu} n_j \frac{\partial v_j}{\partial b_n}\, d\Gamma - \int_\Omega \tilde{\nu}\frac{\partial \tilde{\nu}_a}{\partial x_j}\frac{\partial v_j}{\partial b_n}\, d\Omega + \int_\Gamma \tilde{\nu}_a v_j n_j \frac{\partial \tilde{\nu}}{\partial b_n}\, d\Gamma \\ & \quad - \int_\Omega \frac{\partial \tilde{\nu}_a}{\partial x_j} v_j \frac{\partial \tilde{\nu}}{\partial b_n}\, d\Omega\end{aligned} \tag{14}$$

$$\begin{aligned}term2: \quad & - \int_\Omega \tilde{\nu}_a \frac{\partial}{\partial x_j}\left[\left(\nu + \frac{\tilde{\nu}}{\sigma}\right)\frac{\partial}{\partial x_j}\left(\frac{\partial \tilde{\nu}}{\partial b_n}\right)\right] d\Omega \\ & = - \int_\Gamma \tilde{\nu}_a \left(\nu + \frac{\tilde{\nu}}{\sigma}\right)\frac{\partial}{\partial x_j}\left(\frac{\partial \tilde{\nu}}{\partial b_n}\right) n_j\, d\Gamma + \int_\Gamma \left(\nu + \frac{\tilde{\nu}}{\sigma}\right)\frac{\partial \tilde{\nu}_a}{\partial x_j} n_j \frac{\partial \tilde{\nu}}{\partial b_n}\, d\Gamma \\ & \quad - \int_\Omega \frac{\partial}{\partial x_j}\left[\left(\nu + \frac{\tilde{\nu}}{\sigma}\right)\frac{\partial \tilde{\nu}_a}{\partial x_j}\right]\frac{\partial \tilde{\nu}}{\partial b_n} d\Omega\end{aligned}$$

From Eq. (7) (with $\Phi = \frac{\partial \tilde{\nu}}{\partial x_j}$), we get

$$\frac{\partial}{\partial x_j}\left(\frac{\partial \tilde{\nu}}{\partial b_n}\right) n_j = \frac{\delta}{\delta b_n}\left(\frac{\partial \tilde{\nu}}{\partial x_j} n_j\right) - \frac{\partial \tilde{\nu}}{\partial x_j}\frac{\delta n_j}{\delta b_n} - \frac{\partial^2 \tilde{\nu}}{\partial x_j \partial x_k} n_j \frac{\delta x_k}{\delta b_n}$$

and *term2* is rewritten as

$$\begin{aligned}& - \int_\Omega \tilde{\nu}_a \frac{\partial}{\partial x_j}\left[\left(\nu + \frac{\tilde{\nu}}{\sigma}\right)\frac{\partial}{\partial x_j}\left(\frac{\partial \tilde{\nu}}{\partial b_n}\right)\right] d\Omega \\ & = - \int_\Gamma \tilde{\nu}_a \left(\nu + \frac{\tilde{\nu}}{\sigma}\right)\frac{\delta}{\delta b_n}\left(\frac{\partial \tilde{\nu}}{\partial x_j} n_j\right) d\Gamma + \int_\Gamma \tilde{\nu}_a \left(\nu + \frac{\tilde{\nu}}{\sigma}\right)\frac{\partial \tilde{\nu}}{\partial x_j}\frac{\delta n_j}{\delta b_n}\, d\Gamma \\ & \quad + \int_\Gamma \tilde{\nu}_a \left(\nu + \frac{\tilde{\nu}}{\sigma}\right)\frac{\partial^2 \tilde{\nu}}{\partial x_j \partial x_k} n_j \frac{\delta x_k}{\delta b_n}\, d\Gamma - \int_\Omega \frac{\partial}{\partial x_j}\left[\left(\nu + \frac{\tilde{\nu}}{\sigma}\right)\frac{\partial \tilde{\nu}_a}{\partial x_j}\right]\frac{\partial \tilde{\nu}}{\partial b_n} d\Omega \\ & \quad + \int_\Gamma \left(\nu + \frac{\tilde{\nu}}{\sigma}\right)\frac{\partial \tilde{\nu}_a}{\partial x_j} n_j \frac{\partial \tilde{\nu}}{\partial b_n}\, d\Gamma\end{aligned} \tag{15}$$

$$\begin{aligned}term3: \quad & - \frac{1}{\sigma}\int_\Omega \tilde{\nu}_a \frac{\partial}{\partial x_j}\left(\frac{\partial \tilde{\nu}}{\partial b_n}\frac{\partial \tilde{\nu}}{\partial x_j}\right) d\Omega \\ & = - \frac{1}{\sigma}\int_\Gamma \tilde{\nu}_a \frac{\partial \tilde{\nu}}{\partial x_j} n_j \frac{\partial \tilde{\nu}}{\partial b_n}\, d\Gamma + \frac{1}{\sigma}\int_\Omega \frac{\partial \tilde{\nu}_a}{\partial x_j}\frac{\partial \tilde{\nu}}{\partial x_j}\frac{\partial \tilde{\nu}}{\partial b_n}\, d\Omega\end{aligned} \tag{16}$$

$$\begin{aligned}term4: \quad & - \frac{2c_{b2}}{\sigma}\int_\Omega \tilde{\nu}_a \frac{\partial \tilde{\nu}}{\partial x_j}\frac{\partial}{\partial x_j}\left(\frac{\partial \tilde{\nu}}{\partial b_n}\right) d\Omega = - \frac{2c_{b2}}{\sigma}\int_\Gamma \tilde{\nu}_a \frac{\partial \tilde{\nu}}{\partial x_j} n_j \frac{\partial \tilde{\nu}}{\partial b_n} d\Gamma \\ & \quad + \frac{2c_{b2}}{\sigma}\int_\Omega \frac{\partial}{\partial x_j}\left(\tilde{\nu}_a \frac{\partial \tilde{\nu}}{\partial x_j}\right)\frac{\partial \tilde{\nu}}{\partial b_n} d\Omega\end{aligned} \tag{17}$$

$$\begin{aligned}term5: \quad & \int_\Omega \tilde{\nu}_a \tilde{\nu}\left(-\frac{\partial P}{\partial b_n} + \frac{\partial D}{\partial b_n}\right) d\Omega = \int_\Omega \tilde{\nu}_a \tilde{\nu}\left(\mathscr{C}_S(\tilde{\nu})\frac{\partial S}{\partial b_n} + \mathscr{C}_{\tilde{\nu}}(\tilde{\nu}, \vec{\nu})\frac{\partial \tilde{\nu}}{\partial b_n}\right. \\ & \quad \left. + \mathscr{C}_d(\tilde{\nu}, \vec{\nu})\frac{\partial d}{\partial b_n}\right) d\Omega\end{aligned} \tag{18}$$

where the expressions for functions $\mathscr{C}_s(\tilde{\nu}), \mathscr{C}_{\tilde{\nu}}(\tilde{\nu}, \vec{\nu})$ and $\mathscr{C}_d(\tilde{\nu}, \vec{\nu})$ result directly from the Spalart–Allmaras model equations. Since

$$\frac{\partial S}{\partial b_n} = \frac{1}{S} e_{ijq} e_{ilm}\frac{\partial v_q}{\partial x_j}\frac{\partial}{\partial x_l}\left(\frac{\partial v_m}{\partial b_n}\right) \tag{19}$$

the first term on the r.h.s. of Eq. (18) is rewritten as

$$\int_\Omega \tilde{\nu}_a \tilde{\nu} \mathscr{C}_S(\tilde{\nu}) \frac{\partial S}{\partial b_n} d\Omega = \int_\Gamma \tilde{\nu}_a \tilde{\nu} \mathscr{C}_S(\tilde{\nu}) \frac{1}{S} e_{ijq} e_{ilm} \frac{\partial v_q}{\partial x_j} n_l \frac{\partial v_m}{\partial b_n} d\Gamma - \int_\Omega \frac{\partial}{\partial x_l} \left(\mathscr{C}_S(\tilde{\nu}) \frac{1}{S} e_{ijq} e_{ilm} \frac{\partial v_q}{\partial x_j} \tilde{\nu}_a \tilde{\nu} \right) \frac{\partial v_m}{\partial b_n} d\Omega \quad (20)$$

and

$$term6: \quad \int_\Omega \tilde{\nu}_a (-P + D) \frac{\partial \tilde{\nu}}{\partial b_n} d\Omega. \quad (21)$$

4. Adjoint equations and sensitivity derivatives

The sensitivities of functions expressed as boundary integrals,

$$J = \int_\Gamma J_\Gamma d\Gamma \quad (22)$$

are given by

$$\frac{\delta J}{\delta b_n} = \int_\Gamma \frac{\partial J_\Gamma}{\partial b_n} d\Gamma + \int_\Gamma \frac{\partial J_\Gamma}{\partial x_k} \frac{\delta x_k}{\delta b_n} d\Gamma + \int_\Gamma J_\Gamma \frac{\delta (d\Gamma)}{\delta b_n} \quad (23)$$

where

$$\frac{\partial J_\Gamma}{\partial b_n} = \frac{\partial J_\Gamma}{\partial v_i} \frac{\partial v_i}{\partial b_n} + \frac{\partial J_\Gamma}{\partial p} \frac{\partial p}{\partial b_n} + \frac{\partial J_\Gamma}{\partial \tilde{\nu}} \frac{\partial \tilde{\nu}}{\partial b_n} \quad (24)$$

By substituting Eqs. (12)–(23) into Eq. (6), a lengthy expression for $\frac{\delta L}{\delta b_n}$ can be derived which is omitted in the interest of space. In this expression, integrals which depend on the direct derivatives of the state variables in terms of b_n are eliminated by satisfying the adjoint (mean-flow and turbulence) field equations and their boundary conditions.

Field integrals which include $\frac{\partial v_i}{\partial b_n}$ and $\frac{\partial p}{\partial b_n}$ are eliminated by satisfying the adjoint to the field mean-flow equations,

$$-v_j \left(\frac{\partial u_i}{\partial x_j} + \frac{\partial u_j}{\partial x_i} \right) - \frac{\partial}{\partial x_j} \left[(\nu + \nu_t) \left(\frac{\partial u_i}{\partial x_j} + \frac{\partial u_j}{\partial x_i} \right) \right] + \frac{\partial q}{\partial x_i} \underbrace{- \tilde{\nu} \frac{\partial \tilde{\nu}_a}{\partial x_i} - \frac{\partial}{\partial x_l} \left(e_{jli} e_{jmq} \frac{\mathscr{C}_S}{S} \frac{\partial v_q}{\partial x_m} \tilde{\nu} \tilde{\nu}_a \right)}_{termA1} = 0, \quad i = 1,2,3 \quad (25)$$

$$\frac{\partial u_j}{\partial x_j} = 0 \quad (26)$$

Field integrals which include $\frac{\partial \tilde{\nu}}{\partial b_n}$ give rise to the field turbulent adjoint equation (i.e. a p.d.e. for $\tilde{\nu}$),

$$\frac{\partial \tilde{\nu}_a}{\partial x_j} v_j + \frac{\partial}{\partial x_j} \left[\left(\nu + \frac{\tilde{\nu}}{\sigma} \right) \frac{\partial \tilde{\nu}_a}{\partial x_j} \right] = \frac{1}{\sigma} \frac{\partial \tilde{\nu}_a}{\partial x_j} \frac{\partial \tilde{\nu}}{\partial x_j} + 2 \frac{c_{b2}}{\sigma} \frac{\partial}{\partial x_j} \left(\tilde{\nu}_a \frac{\partial \tilde{\nu}}{\partial x_j} \right) + \tilde{\nu}_a \tilde{\nu} \mathscr{C}_{\tilde{\nu}}(\tilde{\nu}, \vec{v}) + \frac{\delta \nu_t}{\delta \tilde{\nu}} \frac{\partial u_i}{\partial x_j} \left(\frac{\partial v_i}{\partial x_j} + \frac{\partial v_j}{\partial x_i} \right) + (-P + D) \tilde{\nu}_a \quad (27)$$

The adjoint state equations (Eqs. (25) and (26)) and the turbulent adjoint equations are solved using the same segregated scheme used for the state equations (collocated, cell-centered scheme, second-order accuracy). The Spalart–Allmaras equation and its adjoint are solved using fully consistent schemes. For large scale problems, a preconditioned Krylov subspace method (same preconditioner as before) could be used, allowing the solution of the adjoint equations in a small percentage of the time needed to solve the state equations. However, in this paper, CPU cost is not an issue.

In ducted flows, v_i and $\tilde{\nu}$ are fixed and a zero Neumann condition is imposed to the pressure along the inlet boundary Γ_i. Hence, all integrals along Γ_i which include $\frac{\partial v_i}{\partial b_n}$, $\frac{\partial v_t}{\partial b_n}$ (or $\frac{\partial \tilde{\nu}}{\partial b_n}$) and $\frac{\partial}{\partial b_n} \left(\frac{\partial p}{\partial x_j} n_j \right)$ vanish automatically. The remaining integrals along Γ_i are

$$-\int_{\Gamma_i} \phi_{1,ij} \frac{\partial}{\partial x_j} \left(\frac{\partial v_i}{\partial b_n} \right) d\Gamma + \int_{\Gamma_i} \phi_2 \frac{\partial p}{\partial b_n} d\Gamma - \int_{\Gamma_i} \phi_3 \frac{\partial}{\partial b_n} \left(\frac{\partial \tilde{\nu}}{\partial x_j} n_j \right) d\Gamma \quad (28)$$

where

$$\phi_{1,ij} = (\nu + \nu_t)(n_j u_i + n_i u_j), \quad \phi_2 = u_j n_j + \frac{\partial J_\Gamma}{\partial p}, \quad \phi_3 = \tilde{\nu}_a \left(\nu + \frac{\tilde{\nu}}{\sigma} \right)$$

and these are eliminated by setting $\phi_{1,ij} \frac{\partial}{\partial x_j} \left(\frac{\partial v_i}{\partial b_n} \right) = 0, \phi_2 = 0$ and $\phi_3 = 0$. These conditions are equivalent to setting the normal component of the adjoint velocity $\vec{u}$ equal to $-\frac{\partial J_\Gamma}{\partial p}$ and zeroing its tangential components (through a first-order approximation of the zero divergence velocity variation along the walls) as well as $\tilde{\nu}_a$. In addition, the normal derivative of q is set to zero.

Along the outlet boundary Γ_o, integrals which include $\frac{\partial}{\partial b_n} \left(\frac{\partial v_i}{\partial x_j} n_j \right)$, $\frac{\partial p}{\partial b_n}$ or $\frac{\partial}{\partial b_n} \left(\frac{\partial \tilde{\nu}}{\partial x_j} n_j \right)$ vanish due to the exit boundary conditions for the primal mean-flow and turbulence variables. To eliminate

$$\int_{\Gamma_o} \phi_{4,i} \frac{\partial v_i}{\partial b_n} d\Gamma + \int_{\Gamma_o} \phi_5 \frac{\partial \tilde{\nu}}{\partial b_n} d\Gamma \quad (29)$$

where

$$\phi_{4,i} = u_j v_j n_i + u_i v_j n_j + (\nu + \nu_t) \frac{\partial u_i}{\partial x_j} n_j - q n_i + \tilde{\nu}_a \tilde{\nu} n_i + \tilde{\nu}_a \tilde{\nu} \mathscr{C}_S(\tilde{\nu}) \frac{1}{S} e_{jmq} e_{jli} \frac{\partial v_q}{\partial x_m} n_l + \frac{\partial J_\Gamma}{\partial v_i}$$

$$\phi_5 = -\frac{\delta \nu_t}{\delta \tilde{\nu}} u_i \left(\frac{\partial v_i}{\partial x_j} + \frac{\partial v_j}{\partial x_i} \right) n_j + \tilde{\nu}_a v_j n_j + \left(\nu + \frac{\tilde{\nu}}{\sigma} \right) \frac{\partial \tilde{\nu}_a}{\partial x_j} n_j + \frac{\partial J_\Gamma}{\partial \tilde{\nu}}$$

the outlet boundary conditions become $\phi_{4,i} = 0$ (i = 1,2,3 in a 3D problem) and $\phi_5 = 0$. The former corresponds to zeroing the $\vec{\phi}_4$ vector components. So, this is decomposed into its normal and tangential components, as follows:

$$q = u_j v_j + u_n v_n + (\nu + \nu_t) \frac{\partial u_n}{\partial x_j} n_j \underbrace{+ \tilde{\nu}_a \tilde{\nu} + \tilde{\nu}_a \tilde{\nu} \frac{\mathscr{C}_S}{S} e_{jmq} e_{jli} \frac{\partial v_q}{\partial x_m} n_l n_i}_{termA2} + \frac{\partial J_\Gamma}{\partial v_n} \quad (30)$$

$$0 = \vec{u}_t v_n + (\nu + \nu_t) \frac{\partial \vec{u}_t}{\partial x_j} n_j \underbrace{+ \tilde{\nu}_a \tilde{\nu} \frac{\mathscr{C}_S}{S} e_{jmq} e_{jli} \frac{\partial v_q}{\partial x_m} n_l t_i}_{termA3} + \frac{\partial J_\Gamma}{\partial \vec{v}_t} \quad (31)$$

where $v_n = v_i n_i$ (n = normal; t = tangent; no summation over the repeated index n, in Eq. (30)), $\vec{v}_t = \vec{v} - (\vec{v} \cdot \vec{n}) \vec{n}$ and the same holds for the adjoint velocities.

As with the inlet conditions, v_i, $\tilde{\nu}$ and $\frac{\partial p}{\partial x_j} n_j$ are zero along the solid walls Γ_w, too. Since the solid wall is the "controlled" part of the geometry, the corresponding nodal coordinates coincide with or depend on the shape controlling variables and, consequently, the solid wall conditions lead to $\frac{\partial v_i}{\partial b_n} = -\frac{\partial v_i}{\partial x_k} \frac{\delta x_k}{\delta b_n}$, $\frac{\partial}{\partial b_n} \left(\frac{\partial p}{\partial x_j} n_j \right) = -\frac{\partial}{\partial x_k} \left(\frac{\partial p}{\partial x_j} n_j \right) \frac{\delta x_k}{\delta b_n}$ and $\frac{\partial \tilde{\nu}}{\partial b_n} = -\frac{\partial \tilde{\nu}}{\partial x_k} \frac{\delta x_k}{\delta b_n}$. The part of Eq. (6) with boundary integrals along the solid walls becomes

$$\begin{aligned} &\int_{\Gamma_w} \frac{\partial J_\Gamma}{\partial x_k} \frac{\delta x_k}{\delta b_n} d\Gamma + \int_{\Gamma_w} J_\Gamma \frac{\delta (d\Gamma)}{\delta b_n} + \int_{\Gamma_w} J_\Omega \frac{\delta x_k}{\delta b_n} n_k d\Gamma \\ &- \int_{\Gamma_w} \phi_{1,ij} \frac{\partial}{\partial x_j} \left(\frac{\partial v_i}{\partial b_n} \right) d\Gamma + \int_{\Gamma_w} \phi_2 \frac{\partial p}{\partial b_n} d\Gamma - \int_{\Gamma_w} \phi_3 \frac{\partial}{\partial b_n} \left(\frac{\partial \tilde{\nu}}{\partial x_j} n_j \right) d\Gamma \\ &+ \int_{\Gamma_w} \frac{1}{\sigma} \tilde{\nu} \frac{\partial \tilde{\nu}}{\partial x_j} n_j \frac{\partial \tilde{\nu}}{\partial x_k} \frac{\delta x_k}{\delta b_n} d\Gamma + \int_{\Gamma_w} 2 \frac{c_{b2}}{\sigma} \tilde{\nu}_a \frac{\partial \tilde{\nu}}{\partial x_j} \frac{\partial \tilde{\nu}}{\partial x_k} \frac{\delta x_k}{\delta b_n} n_j d\Gamma \\ &+ \int_{\Gamma_w} \tilde{\nu}_a \nu \frac{\partial \tilde{\nu}}{\partial x_j} \frac{\delta n_j}{\delta b_n} d\Gamma + \int_{\Gamma_w} \tilde{\nu}_a \nu \frac{\partial^2 \tilde{\nu}}{\partial x_j \partial x_k} n_j \frac{\delta x_k}{\delta b_n} d\Gamma \\ &- \int_{\Gamma_w} \left[\nu \frac{\partial u_i}{\partial x_j} n_j - q n_i \right] \frac{\partial v_i}{\partial x_k} \frac{\delta x_k}{\delta b_n} d\Gamma - \int_{\Gamma_w} \nu \frac{\partial \tilde{\nu}_a}{\partial x_j} n_j \frac{\partial \tilde{\nu}}{\partial x_k} \frac{\delta x_k}{\delta b_n} d\Gamma \end{aligned} \quad (32)$$

In order to eliminate integrals expressed in terms of $\frac{\partial}{\partial b_n}\left(\frac{\partial v_i}{\partial x_j}n_j\right)$, $\frac{\partial p}{\partial b_n}$ or $\frac{\partial}{\partial b_n}\left(\frac{\partial \tilde{\nu}}{\partial x_j}n_j\right)$, conditions $\phi_{1,ij}\frac{\partial}{\partial x_j}\left(\frac{\partial v_i}{\partial b_n}\right)=0$, $\phi_2=0$ and $\phi_3=0$ should be met. Therefore, from $\phi_3=0$, we get $\tilde{\nu}_a=0$ along the wall and, consequently, any integral containing $\tilde{\nu}_a$ in Eq. (32) vanishes.

Hence, the sensitivity derivatives are given by

$$\frac{\delta J}{\delta b_n}=\int_{\Gamma_w}\frac{\partial J_\Gamma}{\partial x_k}\frac{\delta x_k}{\delta b_n}d\Gamma+\int_{\Gamma_w}J_\Gamma\frac{\delta(d\Gamma)}{\delta b_n}-\int_{\Gamma_w}\left[\nu\frac{\partial u_i}{\partial x_j}n_j-qn_i\right]\frac{\partial v_i}{\partial x_k}\frac{\delta x_k}{\delta b_n}d\Gamma \underbrace{-\int_{\Gamma_w}\nu\frac{\partial\tilde{\nu}_a}{\partial x_j}n_j\frac{\partial\tilde{\nu}}{\partial x_k}\frac{\delta x_k}{\delta b_n}d\Gamma+\int_\Omega\tilde{\nu}_a\tilde{\nu}\mathscr{C}_d(\tilde{\nu},\vec{v})\frac{\partial d}{\partial b_n}d\Omega}_{termB} \tag{33}$$

Working with parameterized curves or surfaces, such as those based on Bézier–Bernstein polynomials, the x_k coordinates along the shape contour are expressed in terms of the non-dimensional parameter t ($t\in[0,1]$) as

$$x_k(t)=\sum_{i=0}^{M-1}C_i(t)X_{ik} \tag{34}$$

($k=1,2,3$ in 3D), M is the number of control points, $C_i(t)$ are appropriate polynomials and X_{ik} are the control point coordinates (some or all of which coincide with the N design variables b_n). The variation in x_k with respect to b_n is

$$\frac{\delta x_k(t)}{\delta b_n}=\sum_{i=0}^{M-1}C_i(t)\frac{\delta X_{ik}}{\delta b_n} \tag{35}$$

The finite length $d\Gamma$ is given by

$$(d\Gamma)^2=(dt)^2\left(\sum_{i=0}^{M-1}\frac{dC_i(t)}{dt}X_{ik}\right)^2 \tag{36}$$

so

$$\frac{\delta(d\Gamma)}{\delta b_n}=\frac{(dt)^2}{d\Gamma}\frac{dx_k(t)}{dt}\left(\sum_{i=0}^{M-1}\frac{dC_i(t)}{dt}\frac{\delta X_{ik}}{\delta b_n}\right) \tag{37}$$

To summarize, by taking into account the variation in ν_t, extra terms appear in the adjoint equations, their boundary conditions and the sensitivity derivatives' expressions. These are clearly marked as *termA*1 (in Eq. (25)), *termA*2 (Eq. (30)), *termA*3 (Eq. (31)) and *termB* (Eq. (33)). Having a clear view of the extra terms and their significance is an important advantage of the continuous adjoint approach. In the case studies, the role of these terms is investigated.

5. Sensitivities of the loss in total pressure – case studies

5.1. Sensitivities of total pressure losses

Thus far, the development was presented in a general form, irrespective of the objective function used. In this section, this is adapted to the case of function J expressing the mass-averaged total pressure losses between the inlet to and outlet from the flow domain (duct or cascade),

$$J=-\int_{\Gamma_i}\left(p+\frac{1}{2}v^2\right)v_in_i\,d\Gamma-\int_{\Gamma_o}\left(p+\frac{1}{2}v^2\right)v_in_i\,d\Gamma \tag{38}$$

Note that the signed integrand J_Γ (see Eq. (22)) is defined only at the inlet and outlet of the domain, where $J_{\Gamma_{i,o}}=\left(p+\frac{1}{2}v^2\right)v_in_i$. Working with Eq. (38), the adjoint boundary conditions become $\vec{u}=0$, $\frac{\partial q}{\partial x_i}n_i=0$ and $\tilde{\nu}_a=0$ along the solid walls, $u_n=v_n,\vec{u}_t=0$, $\frac{\partial q}{\partial x_i}n_i=0$ and $\tilde{\nu}_a=0$ at the inlet and $\phi_{4,i}=0$, with

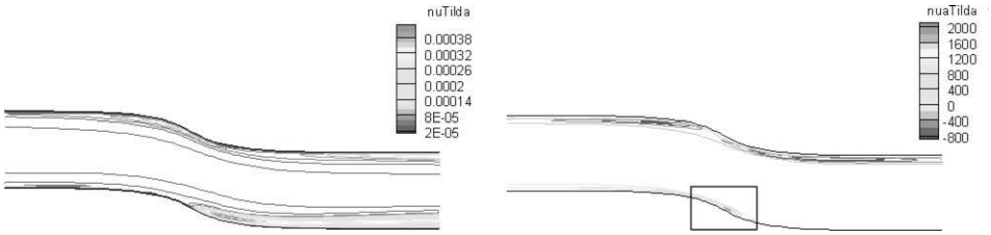

Fig. 1. Case study 1 (S-shaped duct): computed turbulence variable $\tilde{\nu}$ (left) and its adjoint $\tilde{\nu}_a$ fields (right). The latter has been computed using the "full" expression, Eq. (27), proposed in this paper. The rectangle corresponds to the close-up area shown in Fig. 2.

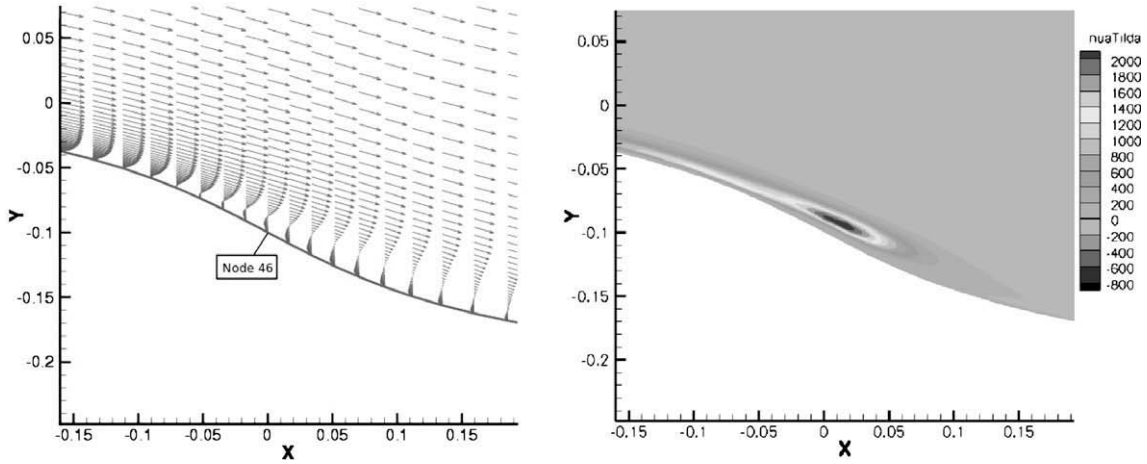

Fig. 2. Case study 1 (S-shaped duct): close-up view of flow and adjoint variables in the divergent part. Left: velocity vectors showing flow separation. Right: adjoint turbulence variable $\tilde{\nu}_a$.

$$\frac{\partial J_\Gamma}{\partial \nu_n} = -\frac{1}{2}v^2 - \nu_n^2, \quad \frac{\partial J_\Gamma}{\partial \vec{\nu}_t} = 0$$

at the outlet. The sensitivity derivatives of J with respect to b_n are expressed by

$$\frac{\delta J}{\delta b_n} = -\int_{\Gamma_w}\left[v\frac{\partial u_i}{\partial x_j}n_j - qn_i\right]\frac{\partial \nu_i}{\partial x_k}\frac{\delta x_k}{\delta b_n}\,d\Gamma \underbrace{-\int_{\Gamma_w} v\frac{\partial \tilde{\nu}_a}{\partial x_j}n_j\frac{\partial \tilde{\nu}}{\partial x_k}\frac{\delta x_k}{\delta b_n}\,d\Gamma + \int_\Omega \tilde{\nu}_a\tilde{\nu}\mathscr{C}_d(\tilde{\nu},\vec{\nu})\frac{\partial d}{\partial b_n}\,d\Omega}_{termB} \quad (39)$$

Three case studies follow in sub Section 5.3. Through them, our aim is to show that the additional use of the adjoint to the turbulence model variable(s) (i.e. the term which is often omitted, to save development and programming time and reduce the CPU cost per optimization cycle) may increase the accuracy of the computed gradient. In contrast, it will be shown that, if the variation in ν_t (or $\tilde{\nu}$) is ignored, the sensitivity derivatives of J, Eq. (39), deviate from the "reference" values. The latter are computed via a direct differentiation method, which is briefly summarized in the next subsection.

5.2. The direct differentiation approach

Direct differentiation is based on the solution of Eqs. (8), (9) and (11) for the sensitivities of the state (mean flow and turbulence) variables. The solution of the aforementioned p.d.e.'s provides the $\frac{\partial \nu_i}{\partial b_n}$, $\frac{\partial p}{\partial b_n}$ and $\frac{\partial \tilde{\nu}}{\partial b_n}$ fields from which the computation of $\frac{\partial J_\Gamma}{\partial b_n}$ is straightforward using Eq. (24). It is also straightforward to set the boundary conditions for the solution variables, based on the corresponding boundary conditions for the state and turbulence variables. So, at the inlet

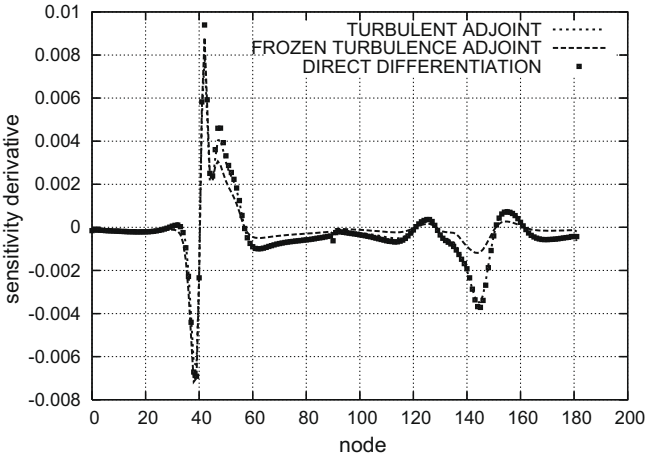

Fig. 3. Case study 1 (S-shaped duct): sensitivity derivatives $\frac{\delta J}{\delta b_n}$, where b_n stand for the normal displacements of the solid wall grid nodes, for the inner wall boundary nodes. The abscissa stands for the nodal numbers. Derivatives are computed using (a) the proposed adjoint method (marked as "turbulent adjoint"), a variant in which the variation in turbulence was neglected (marked as "frozen turbulence adjoint") and direct differentiation.

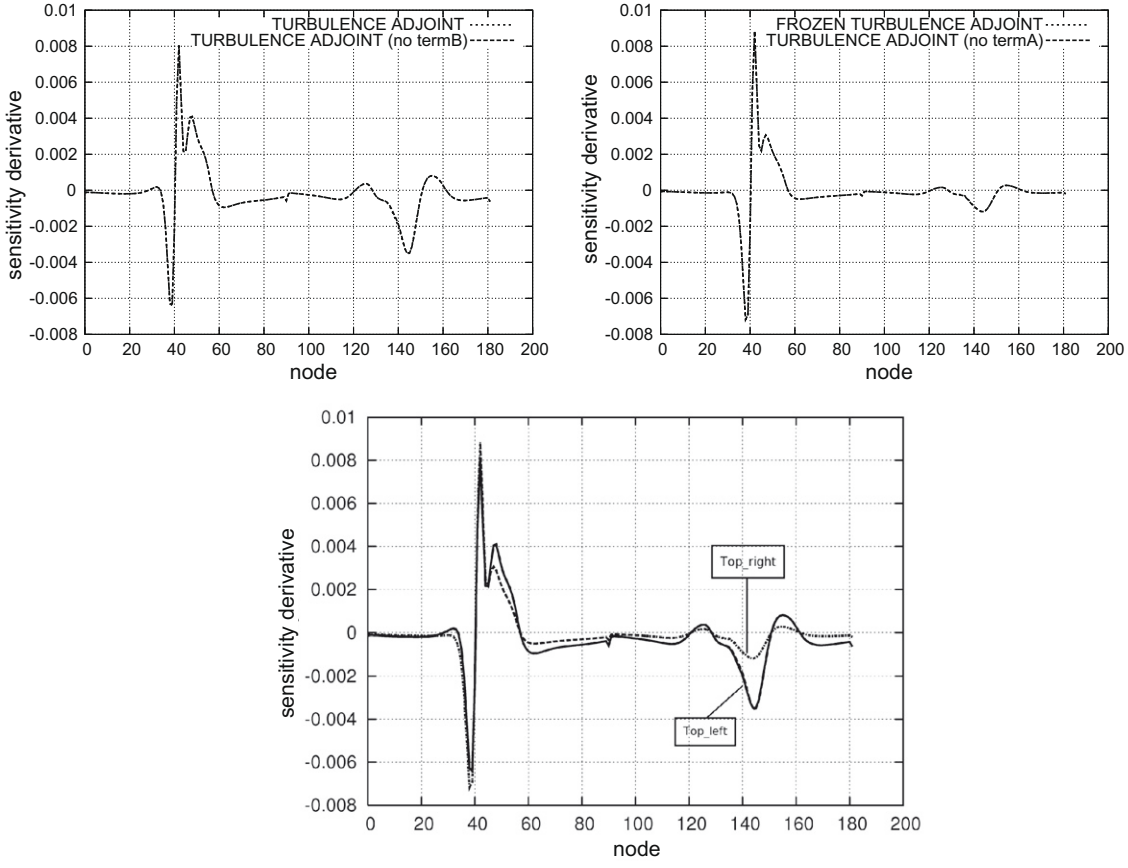

Fig. 4. Case study 1 (S-shaped duct): sensitivity derivatives $\frac{\delta J}{\delta b_n}$. Bottom: Comparison of sensitivities computed using four methods. The four distributions can be paired, yielding two groups of almost coinciding curves as shown separately on the top. Top-left: the proposed method (no terms omission) yields derivatives almost identical to those obtained by omitting *termB* in Eq. (33) or (39). Top-right: derivatives obtained by omitting *termA*1 in Eq. (25) and *termA*2, *termA*3 in Eqs. (30) and (31) are very close to those computed by assuming frozen turbulent viscosity.

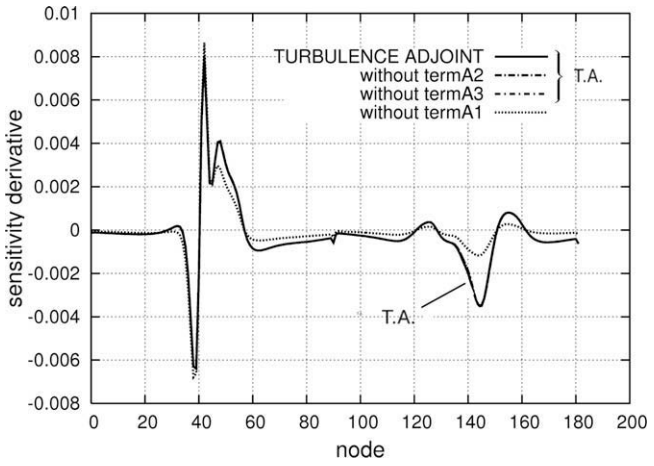

Fig. 5. Case study 1 (S-shaped duct): sensitivity derivatives obtained by the proposed method are compared with those obtained by omitting one term (*termA*1 in Eq. (25) or *termA*2 in Eq. (30) or *termA*3 in Eq. (31)) at a time. The significance of the boundary condition terms (*termA*2 and *termA*3) in the derivatives' accuracy is small (the corresponding distributions and the distribution computed using the full expression practically coincide, yielding the group of three curves marked with T.A.).

$$\frac{\partial v_i}{\partial b_n} = 0, \quad \frac{\partial}{\partial x_j}\left(\frac{\partial p}{\partial b_n} n_j\right) = 0, \quad \frac{\partial \tilde{\nu}}{\partial b_n} = 0 \tag{40}$$

at the outlet

$$\frac{\partial}{\partial x_j}\left(\frac{\partial v_i}{\partial b_n} n_j\right) = 0, \quad \frac{\partial p}{\partial b_n} = 0, \quad \frac{\partial}{\partial x_j}\left(\frac{\partial \tilde{\nu}}{\partial b_n} n_j\right) = 0 \tag{41}$$

and along the solid walls

$$\frac{\partial v_i}{\partial b_n} = -\frac{\partial v_i}{\partial x_k}\frac{\delta x_k}{\delta b_n}, \quad \frac{\partial}{\partial x_j}\left(\frac{\partial p}{\partial b_n} n_j\right) = -\frac{\partial}{\partial x_k}\left(\frac{\partial p}{\partial x_j} n_j\right)\frac{\delta x_k}{\delta b_n}, \quad \frac{\partial \tilde{\nu}}{\partial b_n} = -\frac{\partial \tilde{\nu}}{\partial x_k}\frac{\delta x_k}{\delta b_n} \tag{42}$$

Direct differentiation is computationally expensive since it requires as many field (system of) p.d.e. solutions as the number of shape controlling variables. In this paper, this method is considered to produce the "reference" sensitivity values to compare the outcome of the adjoint approach.

5.3. Case studies – the achieved gain in accuracy

In the first case study, the flow in the S-shaped duct shown in Fig. 1 was considered. The flow was turbulent with a Reynolds number based on the inlet height equal to $Re = 2 \times 10^4$. A structured grid with 200×160 nodes was used; the grid was adequately stretched close to the solid walls to guarantee that the non-dimensional distance of the first nodes off the wall was well below unit (average y^+ of the order of 0.1). All the following results are grid-insensitive. The shape controlling variables, b_n, with respect to which the sensitivity derivatives of J (Eq. (38)) were computed, are the normal displacements of the wall grid nodes. Only, the boundary nodes forming the S-bend section were allowed to

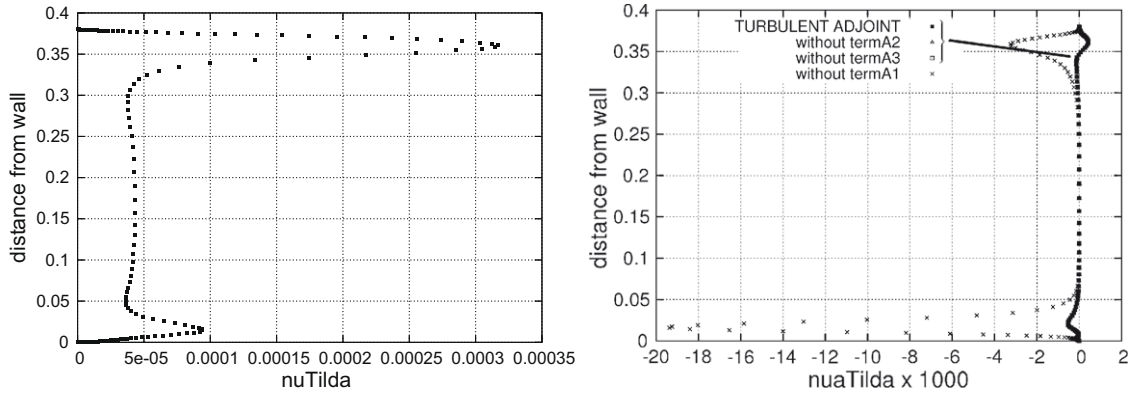

Fig. 6. Case study 1 (S-shaped duct): computed $\tilde{\nu}$ (left) and its adjoint $\tilde{\nu}_a$ (right) profiles along the normal to the inner wall direction at a longitudinal position slightly upstream of the separation. The ordinate is the distance from the inner wall. The $\tilde{\nu}_a$ profiles were computed (a) by the proposed method (b) by omitting *termA*1 in Eq. (25), (c) by omitting *termA*2 in Eq. (30) and (d) by omitting *termA*3 in Eq. (31). Profiles (a), (b) and (c) practically coincide, supporting thus the results presented in Fig. 5.

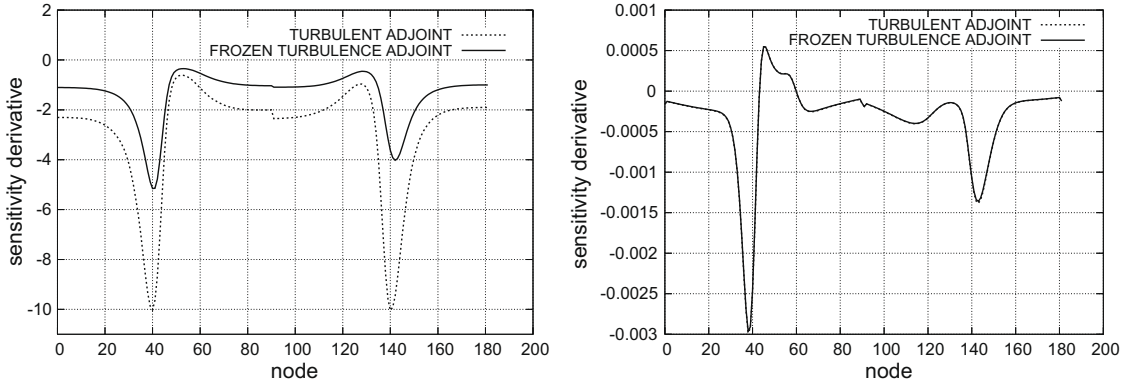

Fig. 7. Case study 1 (S-shaped duct): sensitivity derivatives with respect to nodal normal displacements at two (different than before) Reynolds numbers. Left: $Re = 2 \times 10^5$. Right: $Re = 1000$.

vary; so, derivatives were computed with respect to those points only. The remaining boundary nodes along the straight wall extensions, upstream and downstream of the bend, were fixed. In Fig. 1, the computed turbulence variable $\tilde{\nu}$ and its adjoint $\tilde{\nu}_a$ fields are plotted. Along the divergent part of the duct the flow was separated, as shown in Fig. 2. The same figure clearly shows that $\tilde{\nu}$ takes on high values within the separation zone.

In Fig. 3, the sensitivity derivatives of J, Eq. (38), computed using the proposed and the frozen-turbulence adjoint approaches are shown and compared with the outcome of direct differentiation. In what follows, the term "proposed method" corresponds to the solution of adjoint equations for both the mean-flow and the Spalart–Allmaras equations and the use of Eq. (39) (full expression, including *termB*) to compute the sensitivity derivatives. The proposed method produced sensitivities which are in excellent agreement with the "reference" ones. In contrast, the frozen-turbulence adjoint approach yields derivatives which, in this case, deviate from them.

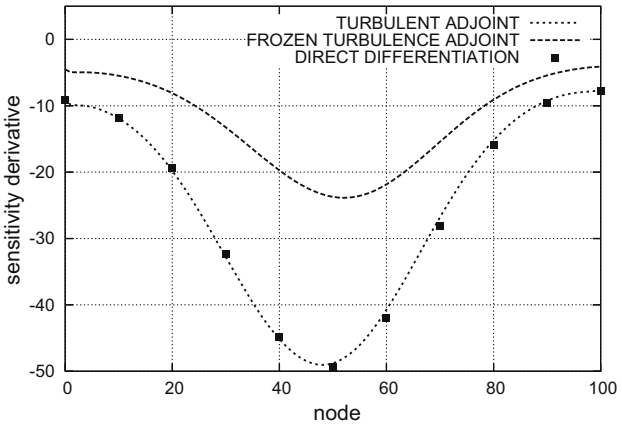

Fig. 8. Case study 2 (duct with bump on its upper wall): sensitivity derivatives $\frac{\delta J}{\delta b_n}$, with respect to the normal displacements of the solid wall grid nodes. Derivatives are computed using the three methods also used in Fig. 3 (same notations).

We below investigate the role of the extra terms appearing in Eqs. (25), (30) and (31) (i.e. the adjoint to the state equations and their boundary conditions) and Eq. (33) (sensitivity derivatives), due to the use of the adjoint to the turbulence equation (terms depending on $\tilde{\nu}_a$). The outcome of this investigation is shown in Fig. 4. From this figure, it is clear that when *termB* in Eq. (33) or (39) was omitted, the sensitivity derivatives remained almost identical to those computed by the proposed method. We thus conclude that terms depending on $\tilde{\nu}$ in the $\frac{\delta J}{\delta b_n}$ expression can safely be omitted, yielding thus significant simplifications. This is an important conclusion since the last term in Eq. (33) or (39) includes the field integral of $\frac{\partial d}{\partial b_n}$ which is a source of computational burden. To compute such a term, each internal grid node must be associated with its distance from the wall and the variations of all these distances must be computed, using for instance, finite differences. Apart from the extra computational cost, the computation of this field integral is a source of numerical error. In contrast, when *termA*1 in Eq. (25) and *termA*2, *termA*3 in Eqs. (30) and (31) were omitted, the resulting derivatives were very close to those computed by freezing the turbulent viscosity and these terms

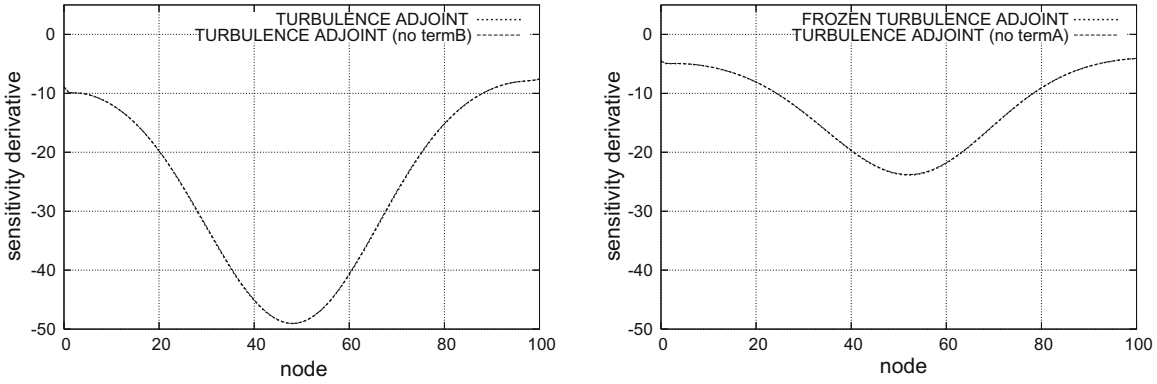

Fig. 9. Case study 2 (duct with bump on its upper wall): sensitivity derivatives as in Fig. 8. Since the vertical axis scaling and bounds are identical, differences between the two pairs of distributions (left and right) can clearly be seen without combining them in a single figure. Captions for the left and right figures are as in Fig. 4.

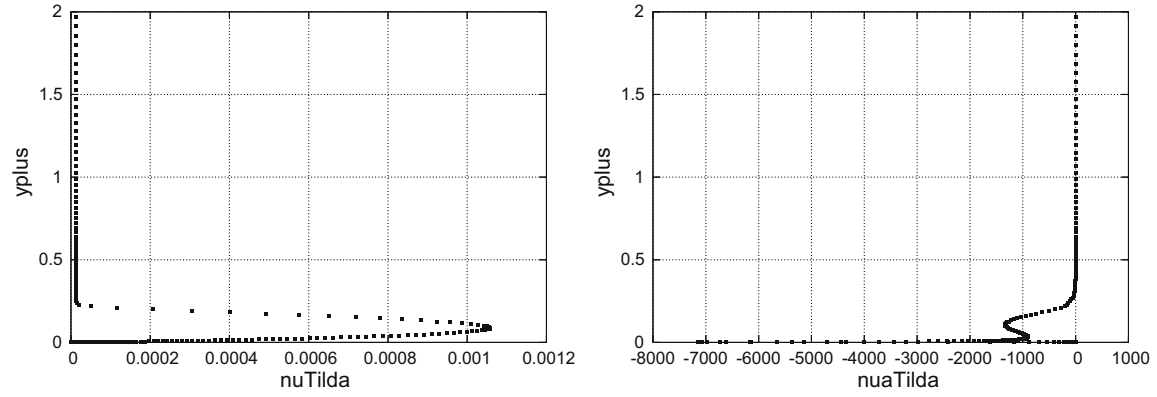

Fig. 10. Case study 2 (duct with bump on its upper wall): computed $\tilde{\nu}$ (left) and its adjoint $\tilde{\nu}_a$ (right) distributions normal to the wall, at the maximum bump height (minimum cross-section). Note that, in this figures, the vertical axis corresponds to the non-dimensional y^+ distance from the wall.

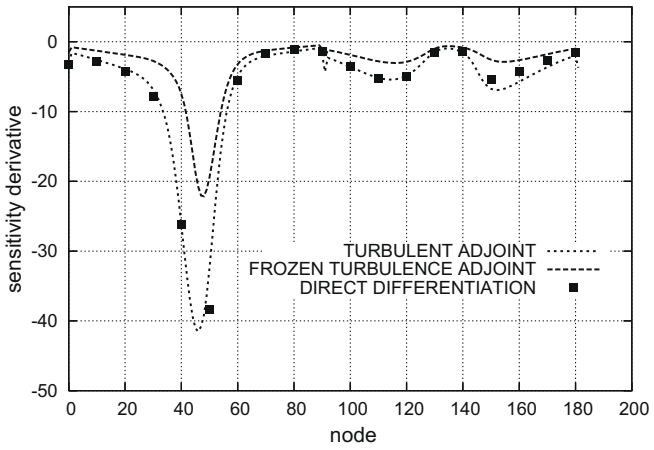

Fig. 11. Case study 3 (90° elbow duct): sensitivity derivatives $\frac{\delta J}{\delta b_n}$, where b_n stand for the normal displacements of the solid wall grid nodes. Derivatives computed using the three methods previously used in Fig. 3 (same notations). The Reynolds number is $Re = 1.2 \times 10^5$.

are, thus, of primary importance for getting highly accurate derivatives.

The previous analysis showed that, if the exact gradient of J is to be computed, it is important to solve the adjoint to the turbulence model equation and use the adjoint turbulent variable $\tilde{\nu}$ in the adjoint to the mean-flow equations and the outlet boundary conditions for the adjoint variables (*termA*1 in Eq. (25), *termA*2 and *termA*3 in Eqs. (30) and (31)). In contrast, *termB* in Eqs. (33) or (39) proved to be non-important at all. To further understand this conclusion, we omitted each one of the three terms (*termA1*, *termA*2 or *termA*3) at a time. From the comparison shown in Fig. 5, it is evident that maintaining *termA*1 in the adjoint to the mean-flow equation is important, even if the outlet adjoint boundary conditions do not include the effect of $\tilde{\nu}_a$.

Fig. 6 shows the transversal profiles of $\tilde{\nu}$ and $\tilde{\nu}_a$ (for the aforementioned four computations) at a longitudinal position slightly upstream of the separation. Only the run in which *termA*1 in Eq. (25) was omitted fails to reproduce the $\tilde{\nu}_a$ transversal distribution computed by the proposed method. In this case, the erroneous overshooting of $\tilde{\nu}_a$ in the vicinity of solid walls affects the solution of the adjoint to the mean-flow equations. Fig. 6 reconfirms the differences observed in Fig. 5.

As shown in Fig. 7, a few extra computations were made to investigate the Reynolds number effect on the predicted sensitivity derivatives. Apart from the previous Reynolds number ($Re = 2\times 10^4$), we re-examined the same case for $Re = 2 \times 10^5$ and $Re = 1000$, by re-adjusting the grids in order to have proper y^+ values at the first nodes off the walls. In the low Reynolds number (which was, however, examined by using the turbulence model) the use or not of the adjoint to the turbulence model equation is irrelevant. In contrast, the frozen turbulence assumption gives quite different derivatives with respect to the present method when the Reynolds number is quite high.

The second case study was concerned with the turbulent flow in a straight duct with a bump. The Reynolds number, based on the inlet height, was equal to 1×10^6. A structured grid with 260×180 nodes was used. Here, also, the b_n are the normal to the solid walls displacements of grid nodes. In Fig. 8, sensitivity derivatives computed using

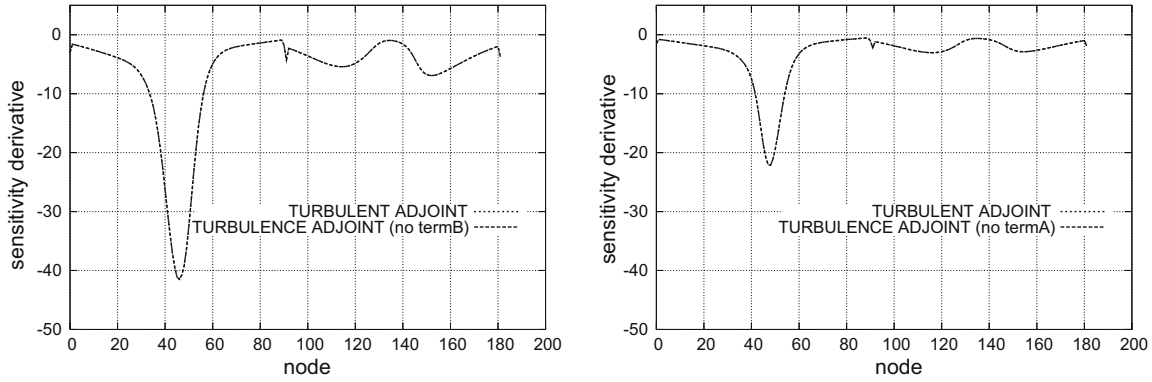

Fig. 12. Case study 3 (90° elbow duct): sensitivity derivatives as in Fig. 11. Since the vertical axis scaling and bounds are identical, differences between the two pairs of distributions (left and right) can clearly be seen without combining them in a single figure. Captions for the left and right figures are as in Fig. 4.

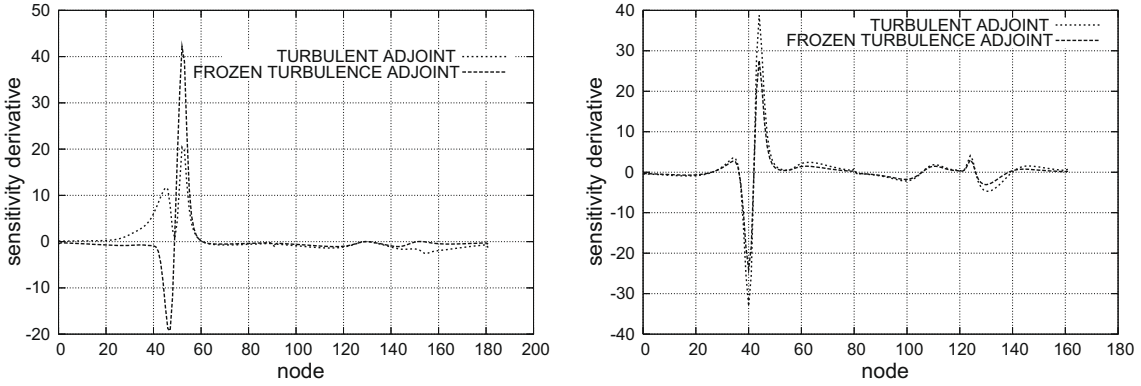

Fig. 13. Case study 3 (90° elbow duct): sensitivity derivatives with respect to nodal normal displacements. Left: $Re = 3.5 \times 10^4$. Right: $Re = 5 \times 10^3$.

the same three methods as in the previous case, are shown. To have a clear picture of the difference among the three methods, only a few consecutive points (nodes) on the abscissa are plotted. The proposed method perfectly matches the outcome of direct differentiation. In contrast, the frozen turbulence assumption leads to considerable underestimation of sensitivity derivatives.

In the same case, we re-investigated the relative importance of the terms introduced in Eqs. (25), (30), (31) and (33) in terms of the adjoint turbulent variable $\tilde{\nu}$, as in the previous case, and the corresponding results are shown in Fig. 9. From this figure, it is confirmed that the omission of *termB* in Eq. (33) does not harm the computed derivatives. Also, the sensitivity derivatives tend to the values produced by the zero turbulent viscosity variation assumption if *termA*1 in Eq. (25) and *termA*2, *termA*3 in Eqs. (30) and (31) were omitted. In this case, the conclusions are the same as in the previous one. In Fig. 10, distributions of $\tilde{\nu}$ and its adjoint $\tilde{\nu}$, along the normal to the wall direction, at the maximum bump height (minimum cross-section) are shown.

Finally, a series or runs on a third geometry, namely a 90° elbow duct with constant cross-section was carried out. One of the purpose of these studies was to re-investigate the Reynolds number effect on the predicted sensitivity derivatives. Three different Reynolds numbers based on the inlet height ($Re = 1.2 \times 10^5$, 3.5×10^4 and 5×10^3) were studied. Here, also, the b_n were the normal to the solid walls displacements of grid nodes, though the computed sensitivities are plotted every 10 grid nodes. In Fig. 11, for $Re = 1.2 \times 10^5$, sensitivity derivatives computed using the same three methods as in the previous cases, are shown. The proposed method perfectly matches the outcome of direct differentiation whereas the frozen turbulence assumption leads to underestimated sensitivity derivatives.

Fig. 12 reconfirms previous findings concerning the role of $\tilde{\nu}$ in the adjoint to the mean-flow equations, the adjoint boundary conditions and the gradient expression. It is shown, once more, that including the two $\tilde{\nu}_a$-depending terms (boundary and field integral) in the gradient expression is almost needless; in contrast, it is important to maintain the $\tilde{\nu}_a$-depending term in the mean-flow equation.

The same runs were repeated twice for the other two Reynolds numbers and these are shown in Fig. 13. From this figure, one may see that (as expected) the frozen turbulence adjoint method deviated much less from the variable turbulent viscosity computation results as the Reynolds number was decreased.

6. Conclusions

A continuous adjoint approach for the complete system of state (mean-flow and turbulence) equations, for incompressible fluid flows, leading to accurate sensitivity derivatives, was presented. The Spalart–Allmaras turbulence model was used to effect closure; other turbulence models could also be used, after deriving the corresponding equations. The presented adjoint formulation may cover the computation of exact sensitivity derivatives for any integral functional. Here, the mass-averaged loss in total pressure was used, the minimization of which is a common objective in internal aerodynamics. Even though the objective function consists of integrals along the inlet and outlet, the sensitivity derivatives are expressed by line/surface integrals along the solid walls, with an additional field integral due to the fact that the Spalart–Allmaras model involves the nodal distances d from the walls. In the examined cases, the shape controlling variables were the normal displacements of the solid wall nodes. However, as shown, the extension to shape parameterization techniques is straightforward.

The gain from the additional use of the adjoint to the turbulence model equation is noticeable if, in particular, a functional that is heavily dependent on turbulence (such the total pressure losses) is used. Compared to "reference" sensitivity derivatives deduced by direct differentiation, the proposed adjoint approach produced almost identical sensitivity derivatives whereas the standard simplification (frozen-turbulence adjoint approach) led to deviations in the gradient values. Based on the examined cases, it was shown that the terms that make this difference appear in the adjoint state equations and their boundary conditions as functions of the adjoint turbulent viscosity. The adjoint turbulent viscosity affects also the expression of the sensitivity derivatives by two extra terms which have negligible effect on the gradient and can, thus, be omitted. This omission is computationally convenient since we omit a term which (a) is the only field integral and (b) depends on $\frac{\delta d}{\delta b_n}$.

Acknowledgments

This research work was funded by Volkswagen AG (Group Research, K-EFFG/V, Wolfsburg, Germany). The first author was supported by a grant from the State Scholarships Foundation, Greece.

References

[1] Pironneau O. On optimum design in fluid mechanics. J Fluid Mech 1974;64:97–110.
[2] Jameson A. Aerodynamic design via control theory. J Sci Comput 1988;3:233–60.
[3] Anderson WK, Venkatakrishnan V. Aerodynamic design optimization on unstructured grids with a continuous adjoint formulation. AIAA Paper, 97-0643; 1997.
[4] Arian E, Salas MD. Admitting the inadmissible: adjoint formulation for incomplete cost functionals in aerodynamic optimization. NASA/CR-97-206269, ICASE Report No. 97-69; 1997.
[5] Hazra S, Schulz V, Brezillon J, Gauger N. Aerodynamic shape optimization using simultaneous pseudo-timestepping. J Comput Phys 2005;204(1):46–64.
[6] Papadimitriou D, Giannakoglou K. A continuous adjoint method with objective function derivatives based on boundary integrals for inviscid and viscous flows. Comput Fluids 2007;36:325–41.
[7] Othmer C. A continuous adjoint formulation for the computation of topological and surface sensitivities of ducted flows. Int J Numer Methods Fluids 2008;58(8):861–77.
[8] Shubin GR, Frank PD. A comparison of the implicit gradient approach and the variational approach to aerodynamic design optimization. Boeing computer services report AMS-TR-163; 1991.
[9] Burgreen GW, Baysal O. Three-dimensional aerodynamic shape optimization using discrete sensitivity analysis. AIAA J 1996;34(9):1761–70.
[10] Elliot J, Peraire J. Aerodynamic design using unstructured meshes. AIAA Paper, 96-1941; 1996.
[11] Duta MC, Giles MB, Campobasso MS. The harmonic adjoint approach to unsteady turbomachinery design. Int J Numer Methods Fluids 2002;40(3–4):323–32.
[12] Jameson A, Pierce N, Martinelli L. Optimum aerodynamic design using the Navier–Stokes equations. Theor Comput Fluid Dyn 1998;10:213–37.
[13] Mohammadi B, Pironneau O. Applied shape optimization for fluids. Oxford: Clarendon Press; 2001.
[14] Jameson A, Kim S. Reduction of the adjoint gradient formula in the continous limit. AIAA Paper, 2003-0040; 2003.
[15] Soto O, Lohner R. On the computation of flow sensitivities from boundary integrals. AIAA Paper, 2004-0112; 2004.
[16] Papadimitriou DI, Giannakoglou KC. Total pressure losses minimization in turbomachinery cascades using a new continuous adjoint formulation. Proc Inst Mech Eng A 2007;222(6):865–72.
[17] Papadimitriou DI, Giannakoglou KC. A continuous adjoint method for the minimization of losses in cascade viscous flows. AIAA Paper, 2006-0049; 2006.
[18] Papadimitriou DI, Giannakoglou KC. Compressor blade optimization using a continuous adjoint formulation. ASME TURBO EXPO, GT2006/90466, Barcelona; 2006.
[19] Spalart P, Allmaras S. A one-equation turbulence model for aerodynamic flows. AIAA Paper, 92-0439; 1992.
[20] Giles MB, Pierce NA. Adjoint equations in CFD: duality, boundary conditions and solution behaviour. AIAA Paper, 97-1850; 1997.
[21] Giles MB, Pierce NA. An introduction to the adjoint approach to design. In: ERCOFTAC workshop on adjoint methods, Toulouse, 21–23 June 1999.
[22] Anderson WK, Bonhaus DL. Airfoil design on unstructured grids for turbulent flows. AIAA J 1999;37(2):185–91.
[23] Nielsen EJ, Lu J, Park MA, Darmofal DL. An implicit exact dual adjoint solution method for turbulent flows on unstructured grids. Comput Fluids 2004;33:1131–55.
[24] Lee BJ, Kim C. Automated design methodology of turbulent internal flow using discrete adjoint formulation. Aerosp Sci Technol 2007;11:163–73.

[25] Zingg DW, Leung TM, Diosady L, Truong AH, Elias S, Nemec M. Improvements to a Newton–Krylov adjoint algorithm for aerodynamic optimization. AIAA Paper, 2005-4857, 2005.
[26] Dwight RP, Brezillon J. Effect of approximations of the discrete adjoint on gradient-based optimization. AIAA J 2006;44(12):3022–31.
[27] Mavriplis DJ. Discrete adjoint-based approach for optimization problems on three-dimensional unstructured meshes. AIAA J 2007;45(4):740–50.
[28] Kim CS, Kim C, Rho OH. Feasibility study of constant eddy-viscosity assumption in gradient-based design optimization. J Aircraft 2003;40(6):1168–76.
[29] Caretto LS, Gisman AD, Patankar SV, Spalding DB. Two calculation procedures for steady three-dimensional flows with recirculation. In: Proceedings of the third international conference on numerical methods in fluid dynamics, Paris; 1972.
[30] Saad Y. Iterative methods for sparse linear systems. Electronic Edition (copyright by Y. Saad); 2000.
[31] Nadarajah SK, Jameson A. Studies of the continuous and discrete adjoint approaches to viscous automatic aerodynamic shape optimization. AIAA Paper, 2001-2530; 2001.